Experimental Analysis of the Magnetic Properties of the Kagome System $YBaCo_3FeO_7$

Bastian Marschner

Supervised by A/Prof. C. Ulrich

Research Findings Report

November 2024

School of Physics

Faculty of Science

The University of New South Wales

1. Abstract

Highly frustrated spin quantum systems have recently become a key area of research in the field of condensed matter physics. In such systems, spins may not order to form a traditional magnetic state even down to very low temperatures, due to a variety of prohibiting factors. Most notably, the geometry of a triangular and/or hexagonal lattice comprising a given material can make it geometrically impossible for spins to order properly.

The swedenborgite compound $YBaCo_3FeO_7$ is one such material and has been hypothesized to behave as a spin liquid by W. Schweika [1], thus closely resembling a paramagnetic high-temperature state even near absolute zero. Though long-range order is never achieved, local ordering eventually takes place at low temperatures and appears remarkably stable. A Fourier analysis revealed that "within the surprisingly large observable range of correlations, the structure appears as an inhomogeneous magnetic state consisting of multiple… zero dimensional entities in a random rather than ordered fashion" [1]

The aim of this project was to determine the magnetic properties of this highly interesting spin frustrated material by SQUID magnetization measurements. After confirming the existing magnetization measurements, the focus of this experiment was to analyze the magnetic hysteresis within the given material as this can help understand the fundamental magnetic properties. For example, if there is a true lack of order resembling the paramagnetic state, no hysteresis arises. Likewise, if a small hysteresis is observed, this can indicate some short-range ordering, depending of course on the size and shape of the phenomenon.

A hysteresis loop is a materials altering response to changes in an external magnetic field. Specifically, a material may exhibit different magnetic moments at the same applied magnetic field based on past events. During the magnetometer experiments conducted by Valldor et al. in 2011 [2], weak hysteresis loops have been observed when applying small external fields (up to 0.2T) using a crystalline sample. It is noteworthy that this experiment only observed hysteresis loops with the external field applied parallel to the crystallographic c-axis, i.e. perpendicular to the a-b plane where the spins are located, with no remarkable hysteresis seen when the magnetic field was applied in the plane of the spins, the ab-pane. A further analysis using stronger external fields at low temperatures may definitively reveal the magnetic behavior of the compound. To experimentally verify and extend the findings of Valldor et al., including a thorough analysis of the hysteresis, will be the aim of this investigation. Therefore, we have performed highly sensitive SQUID magnetization measurements at significantly higher magnetic fields, i.e. from -7 T to +7 T, and have extended the temperature range of the experiment down to 2 K. The obtained results will thus be contributing to a better understanding of the material system in question.

Table of Contents

2.1 Electromagnetism *4*

2.2 Electron Spin & Types of Magnetism *5*

2.3 Magnetic Frustration *7*

2.4 Hysteresis *8*

3.1 Magnetometers & SQUID *9*

3.2 Procedure *10*

4. Results *11*

5.1 Conclusion *17*

5.2 Outlook *17*

References *19*

2.1 Electromagnetism

Since ancient times, human civilizations have utilized the properties of magnetic materials to advance science and technology. The discovery of the first magnetic compass in 206 BC played a key role in helping Chinese and later European sailors navigate the oceans and explore new territories from the 11th century onward. However, it was not until 1820 that the Danish scientist H. C. Oersted discovered the connection between magnetism and electric current, paving the way for various innovations including the electric motor [3].

According to Oersted, whenever an electric charge of any magnitude is in motion, this results in a magnetic field which impacts nearby charges within its radius of influence by exerting a force. Specifically, the movement of a charged particle will result in a vector field, where each point in space corresponds to a force vector comprised of a magnitude and a direction [3]. For this investigation, a magnetic field will either be measured in Tesla (T) or Oersted (Oe), which are distinct quantities, as a Tesla is defined as the resulting field within the medium whereas an Oersted represents the applied field from the source.

At the points where the magnitude of the magnetic field is greatest, so-called "North" and "South" poles are formed. These poles point in opposite directions and always emerge as a pair in what is known as a magnetic dipole. It is thus never possible to create a North pole without simultaneously creating a South pole and vice versa.

Maxwell's four well-known equations provide a great overview of these findings while also serving as the foundation of electromagnetism as it is known today. Maxwell's equations are:

$$(1)\ \nabla \cdot \mathbf{E} = \frac{\rho}{\varepsilon_0}$$

$$(2)\ \nabla \cdot \mathbf{B} = 0$$

$$(3)\ \nabla \times \mathbf{E} = -\frac{\delta \mathrm{B}}{\delta t}$$

$$(4)\ \nabla \times \mathbf{B} = \mu_0 \cdot (\mathbf{J} + \varepsilon_0 \frac{\delta \mathrm{E}}{\delta t})$$

Where:

- **E** is the electric field,
- **B** is the magnetic field,
- **J** is the current density,
- ρ is the electric charge density,
- ε_0 is the permittivity of free space,
- μ_0 is the permeability of free space.

Equation (1) states that the total electric flux passing out of any closed surface is proportional to the total electric charge enclosed within that surface

Equation (2) implies that magnetic monopoles (isolated north or south magnetic poles) do not exist, meaning that the north pole of a magnet will be equally strong as the south pole (so the sum of the flux is zero)

Equation (3) describes the relationship between the induced electromotive force and the rate of change of the magnetic field that caused it. The electromotive force and the magnetic field always act in opposite directions.

Equation (4) describes how both electric currents and changing electric fields produce magnetic fields. The $\frac{\delta \mathrm{E}}{\delta t}$ term accounts for situations without physical current, such as in a capacitor, where the changing electric field still creates a magnetic field.

Over the coming centuries, many powerful applications of these equations would become apparent. Particularly noteworthy is the cyclical relationship between an electric and a magnetic field, where one always induces the other, which explains how electromagnetic waves can keep travelling through space indefinitely.

2.2 Electron Spin & Types of Magnetism

During the early 1920's, the scientists O. Stern and W. Gerlach performed an experiment that eventually led to the discovery of the electron "spin" [4]. Spin was found to be an intrinsic property all electrons possess as a direct consequence of quantum mechanics rather than any physical rotation of the electrons. An electron's spin is represented by the vector **S** and either points "up" (spin = ½) or "down" (spin = -½). Up and down are defined relative to an external magnetic field, where spin parallel to the external field lined denotes spin up, and spin anti-parallel to the external field lines denotes spin down. In the spin-up state, electrons gain energy in an external magnetic field, $E_{mag} = \mu_B B$ where μ_B is the Bohr magneton, $\mu_B = \frac{e\bar{h}}{2m_e}$.

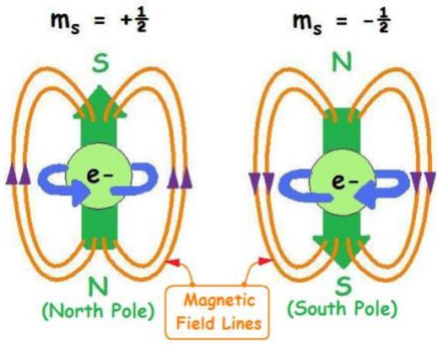


Figure 2.2.1: *Graphical representation of spin up (left) and spin down (right) with an external magnetic field applied [4].*

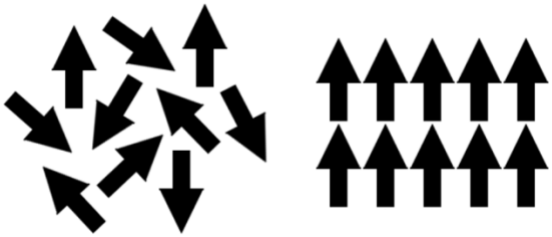


Figure 2.2.2: Free *spin alignment in paramagnetic material without (left) and with external magnetic field applied.*

This implies that not only the movement of electrons, but electrons themselves create a small magnetic field, called magnetic moment. The field arises from an electron's spin properties and is thus always aligned with the electron's spin vector. This allows for the direct interaction of electrons with external magnetic fields. Materials are categorized into five classical magnetic states, depending on how electron spins behave when an external field is applied [5]:

In **diamagnetic** materials, all electron spins are paired (pointing in opposite directions), resulting in no net magnetization. When an external field is applied, diamagnetic compounds are repelled, since the field induces a small temporary magnetic moment in the opposite direction. Examples of diamagnetic materials include copper, gold and water.

In **paramagnetic** materials, unpaired electrons exist but spins lack any alignment without the presence of an external magnetic field, resulting in no magnetic moment. When exposed to an external field, free electron spins typically align parallel to the field, creating a weak attractive force. Examples of paramagnetic materials include aluminum, platinum and some salts.

In **ferromagnetic** materials, unpaired electrons exist, and spins align parallel to each other in magnetic domains (regions where spins point in the same direction). When subjected to a strong external magnetic field, domains tend to align in the same way and remain this way even after the magnetic field is removed, meaning that the material now exerts a permanent magnetic field itself. Above a certain ordering temperature, the Curie temperature T_c the spins become misaligned, and the material becomes paramagnetic. Examples of ferromagnetic materials include iron, cobalt and nickel.

In **antiferromagnetic** materials, unpaired electrons exist but spins align in opposite direction to their neighboring spins when an external field is applied, effectively cancelling any net magnetic moment. Substances are antiferromagnetic below a certain ordering temperature, the Neel temperature T_n above which they too become paramagnetic. Examples of antiferromagnetic materials include manganese oxide and iron oxide.

In **ferrimagnetic** materials, spins too align alternatingly in opposite directions but with unequal magnitudes, resulting in partial magnetization even without an external field as in the case of a ferromagnet. Examples of ferrimagnetic materials include trevorite, magnetite and magnesioferrite.

Evidently, a material can adopt multiple magnetic orders depending on the temperature, as is indeed the case with most substances. However, some form of order will typically form when a substance is sufficiently cooled, with the paramagnetic state only present at higher temperatures.

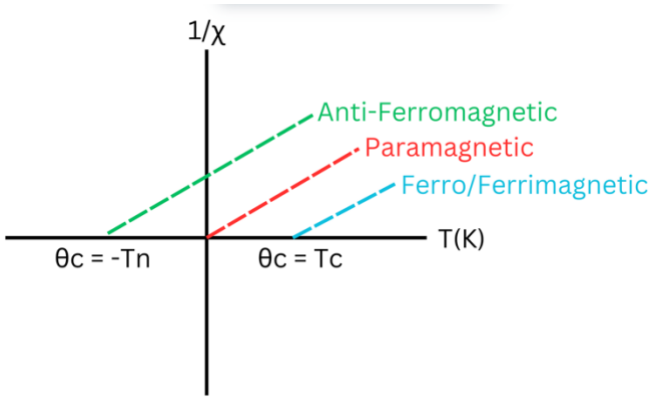


Figure 2.2.3: *Simplified schematic of a Curie-Weiss plot.* $\boldsymbol{\theta_c}$ *is equal to* $\boldsymbol{T_c}$ *in ferro/ferrimagnetic materials, while* $-\boldsymbol{\theta_c} = \boldsymbol{T_N}$ *in antiferromagnetic materials. A phase transition to the paramagnetic state typically occurs close to* $\boldsymbol{T_c}$ *and* $\boldsymbol{T_N}$ *respectively, unless other quantum phenomena are involved.*

To examine temperature-dependent transitions between magnetic states, the Curie-Weiss law provides a very convenient analysis. The Curie-Weiss law is given by:

$$\chi = \frac{C}{T - \theta_c}$$

Where:

- χ is the magnetic susceptibility,
- **C** is the Curie constant,
- θ_c is the Curie-Weiss temperature of a given material.

In most materials, the Curie-Weiss temperature, θ_c closely matches the transition temperature into the paramagnetic state, unless some significant quantum interactions interfere. The Curie-Weiss temperature is found by plotting $1/\chi$ with respect to temperature and extrapolating the intersection with the horizontal axis. If the intersection point is negative, this indicates an anti-ferromagnetic material, which would adopt the paramagnetic state above the Néel temperature T_N, approximated by $|\theta_c|$. Likewise, if the intersection point is positive, a paramagnetic state is expected above the Curie temperature T_c which is approximated by θ_c.

2.3 Magnetic Frustration

In reality, not all materials are able to order in one of the five magnetic states described above. Competing quantum interactions as well as geometric frustration due to the crystallographic structure of certain substances can make it difficult to impossible for spins to order. In the material system present, geometric frustration is indeed very pronounced, as the crystal structure resembles the well-studied pyrochlore lattice [1]. The magnetic ions (Co and Fe) are arranged into tringles which form the basis for the hexagonal pattern of a single crystal layer.

Figure 2.3.1 (a) shows a single triangle, where the first two spins, left and top are antiferromagnetically aligned. The third spin would be e.g. ferromagnetically aligned to the top spin and antiferromagnetically aligned to the left spin, which is antagonistic. As consequence

various spin structures are possible - all pointing inwards as shown in Figure 2.3.1 (b) or pointing in a circle. Both solutions would be energetically unfavorable. In the most extreme case, spins would not order at all, down to lowest temperatures, forming a spin liquid, or a spin glass, where they are frozen in random orientations.

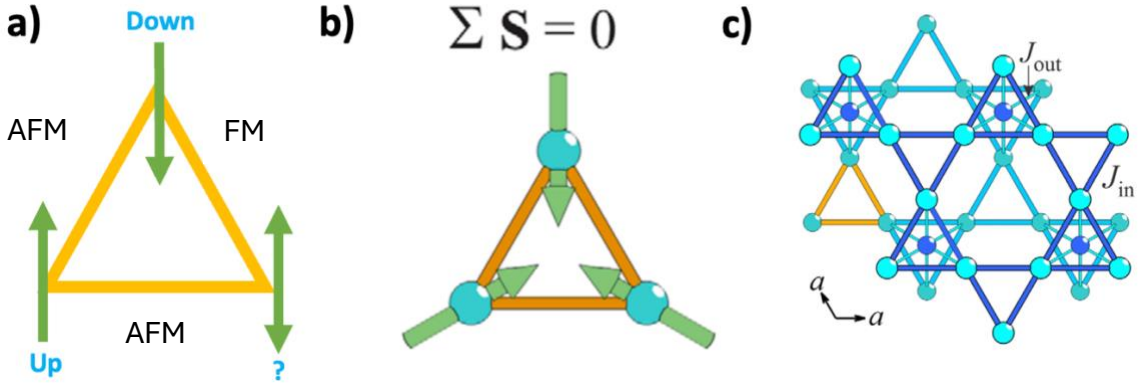


Figure 2.3.1: *Geometrical frustration arises from lattice structure. (a) shows the lack of perfect solutions for spin ordering. (b) shows a potential solution, with all spins pointing inwards, though this means are no longer parallel or antiparallel to each other, but instead at a 120-degree angle [1]. (c) shows how the triangles are arranged in the hexagonal lattice of the crystal [1].*

2.4 Hysteresis

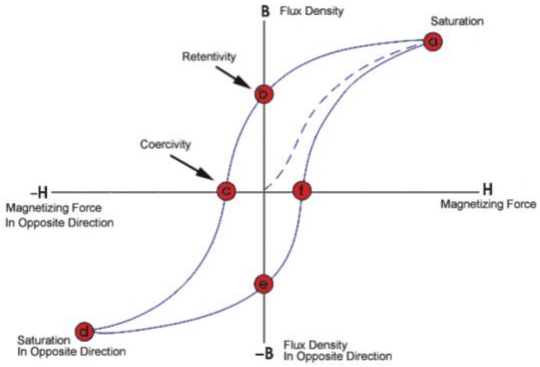


Figure 2.4.1: *Graphical representation of a hysteresis loop. This shape is typical for a hysteresis loop, where the largest difference between the upper and lower recorded magnetic moment is seen at the origin. This difference converges towards the points of highest external magnetization [6].*

Hysteresis loops are graphical representations of the alternating magnetic response of a material when subjected to an external field. Particularly, hysteresis analysis allows for a closer examination of phenomena such as coercivity (the resistance to demagnetization), remanence (residual magnetization after the field is removed), and the magnetic saturation point. These characteristics reveal important details about the material's internal magnetic interactions, such as how strongly magnetic domains resist alignment or realignment [7].

The area of the hysteresis measures the energy lost per cycle due to internal friction between the spins and is found by $\boldsymbol{W = \int H\, dB}$ [7]. In a paramagnetic state, this area would be zero, as spins are free to align in any direction, resulting in negligible friction. A small hysteresis would indicate the existence of small short-range spin-spin interactions in the predominantly disordered paramagnetic phase.

In the case of $YBaCo_3FeO_7$, hysteresis measurements can indicate whether the material exhibits spin-glass or spin-liquid like behavior or other forms of magnetic ordering at low temperatures. A broad loop with low remanence and high coercivity would suggests that spins find it more difficult to align with the magnetic field, which could support the theory of localized order at low temperatures. Additionally, temperature-dependent changes in the hysteresis help with mapping phase transitions and understanding the degree of frustration in the lattice. Though hysteresis loops have been observed in the given material system, they have never been examined with a high external magnetic field (up to 70,000 Oe) and systematically at low temperatures. Furthermore, their shape and size has never been closely analyzed, which is why they will be a key aspect of this investigation.

3.1 Magnetometers & SQUID

To experimentally analyze the magnetic properties of a given material, it's response to an external applied field must be measured. This response is called magnetic susceptibility $\boldsymbol{\chi}$, and is simply the ratio of a material's magnetization divided by the strength of this field. Clearly, the more accurate an instrument can measure the magnetization of a material, the more accurate the experimental analysis.

Early magnetometers, such as the Gauss meter, were simple devices primarily designed to detect the Earth's magnetic field. As technology advanced, more sophisticated instruments like the vibrating-sample magnetometer (VSM) were introduced [8]. In a VSM, a sample vibrates within a magnetic field, and the induced voltage in pickup coils enables a more precise measurement of its magnetic moment. This method significantly enhanced sensitivity and facilitated detailed studies of magnetic susceptibility, hysteresis, and coercivity. However, as researchers sought to investigate more subtle magnetic phenomena and study materials at smaller scales, they required devices with even greater precision and sensitivity.



Figure 3.1.1: *Picture of the front-facing side of the MPMS3 SQUID used for this experiment [9].*

Quantum Design MPMS3 Specifications	
Sensitivity:	$< 5 \cdot 10^{-8}$ emu
Temperature Range:	1.8K – 400K
Temperature Accuracy:	$\pm$ 1%
Temperature Stability:	$\pm$ 0.5%
Magnetic Field Range:	$\pm$ 70,000 Oe
Magnetic Field Resolution:	0.33 Oe
Magnetic Field Remnant:	4.87 Oe
Cooling:	Liquid Helium

Figure 3.1.2: *Selection of the typical specifications of an MPMS3 as stated by Rev [9].*

The introduction of superconducting quantum interference devices (SQUIDs) represented a significant advancement in magnetometry. SQUIDs operate based on superconducting loops with Josephson junctions, which possess exceptional sensitivity to changes in magnetic flux, enabling them to detect even smaller magnetic fields. This unparalleled sensitivity has led to widespread adaptation of SQUID magnetometers for studying the magnetic properties of materials under extreme conditions, such as low temperatures and low external magnetic fields. Researchers can now investigate quantum-level effects and complex magnetic behaviors, including antiferromagnetism, spin glass states, and the elusive spin liquid phase.

For this experiment, a quantum design MPMS3 will be used as the primary instrument to collect data. Though the general specifications are listed in figure 6.2 above, the MPMS3 is highly configurable and usually custom-built for each laboratory setup.

3.2 Procedure

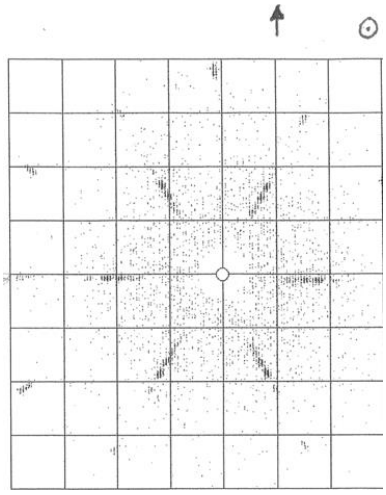


Figure 3.2.1: *X-ray Laue image of the a-b plane used to align the crystal. The hexagonal lattice can be seen clearly, and Bragg peaks are sharp and symmetric, showing the excellent crystal quality.*

The crystal used for analysis was grown by Valldor et al. using the same method as described in Rev [10] and [11] and oriented by W. Schweika using the X-Ray Laue image shown in figure 7.1. The image shows the Bragg peaks of the crystal in the **a-b** plane, where **a** denotes the horizontal and **b** the vertical axis, while the **c**-axis denotes the normal to the **a-b** plane. Measurements were conducted in three different orientations, with the external magnetic field applied parallel to **c** ($\boldsymbol{B}||\boldsymbol{c}$), parallel to ***a*** ($\boldsymbol{B}||\boldsymbol{a}$ *and* $\boldsymbol{B}\perp\boldsymbol{c}$) and parallel to **b** ($\boldsymbol{B}||\boldsymbol{b}$ *and* $\boldsymbol{B}\perp\boldsymbol{c}$). These orientations will hereon be referred to as parallel, perpendicular [1] and perpendicular [2] respectively.

All measurements were conducted by placing the sample in the sample chamber using the correct orientation and running a script on the MPMS3. The raw data was saved in numerous .dat files and subsequently analyzed in Origin 8.5.

For the temperature-dependent measurements, the material was first heated to 400K before each run, to "melt" any remaining magnetic formations from lower temperatures. The probe was then cooled or heated from the initial to the final temperature, while measuring the magnetic moment at the respective temperature intervals in between. Though the MPMS3 has a maximum ramp rate of 300K to 2.8K in 25 minutes, a ramp rate of approximately 3.5 hours was chosen instead to allow temperatures to stabilize and ensure the most accurate results. This was repeated with no external field, 100Oe external field and 1000Oe external field applied, at all three orientations.

For the hysteresis measurements, the material was again heated to 400K before being cooled to the respective temperature. The external magnetic field was then increased linearly to 70000Oe before dropping to -70000Oe and finally returning to 70000Oe, with the magnetic moment of the material measured at each interval and the whole process taking approximately 3 hours. This was again repeated for a variety of temperatures and in all three different orientations, although only a single measurement at 15K was possible in the second perpendicular orientation.

4. Results

For the vast amount of output obtained from the SQUID to be processed, the raw data was first organized into a file table before being processed for interpretation. For a first overview of the findings, Figure 4.1 was constructed, where the top two graphs are a simple plot of the temperature-dependent change in magnetic moment at three different applied fields (scaled for readability where applicable).

The broad transition at 50K is immediately obvious and matches the results obtained in the past [1]. The smaller transition at around 300K, though much less pronounced, also verifies existing measurements. The proposed spin liquid ground state could therefore be a viable characterization for the mate Interestingly, both transitions are much more distinct in the

perpendicular [1] orientation, which was not expected, as the high-temperature transition at 590K observed by Valldor is only visible in the parallel orientation.

The lower graph shows a temperature-dependent approximation of the area between the higher and the lower magnetic moment of the hysteresis. This was obtained by fitting a fifth-degree polynomial to trace both curves, and then integrating between them. The hysteresis is strongest in the 15K-20K temperature range, from which point on it rapidly diminishes. Again, 50K is noteworthy as it represents the starting point from which on the area begins to become significant, at least in the parallel orientation. The perpendicular [1] orientation yields a greater peak area (matching the sharper transitions observed) but showcases a similar overall behavior, at least up to 40K. Measurements above 40K could not be conducted due to time constraints but would be of interest in the future.

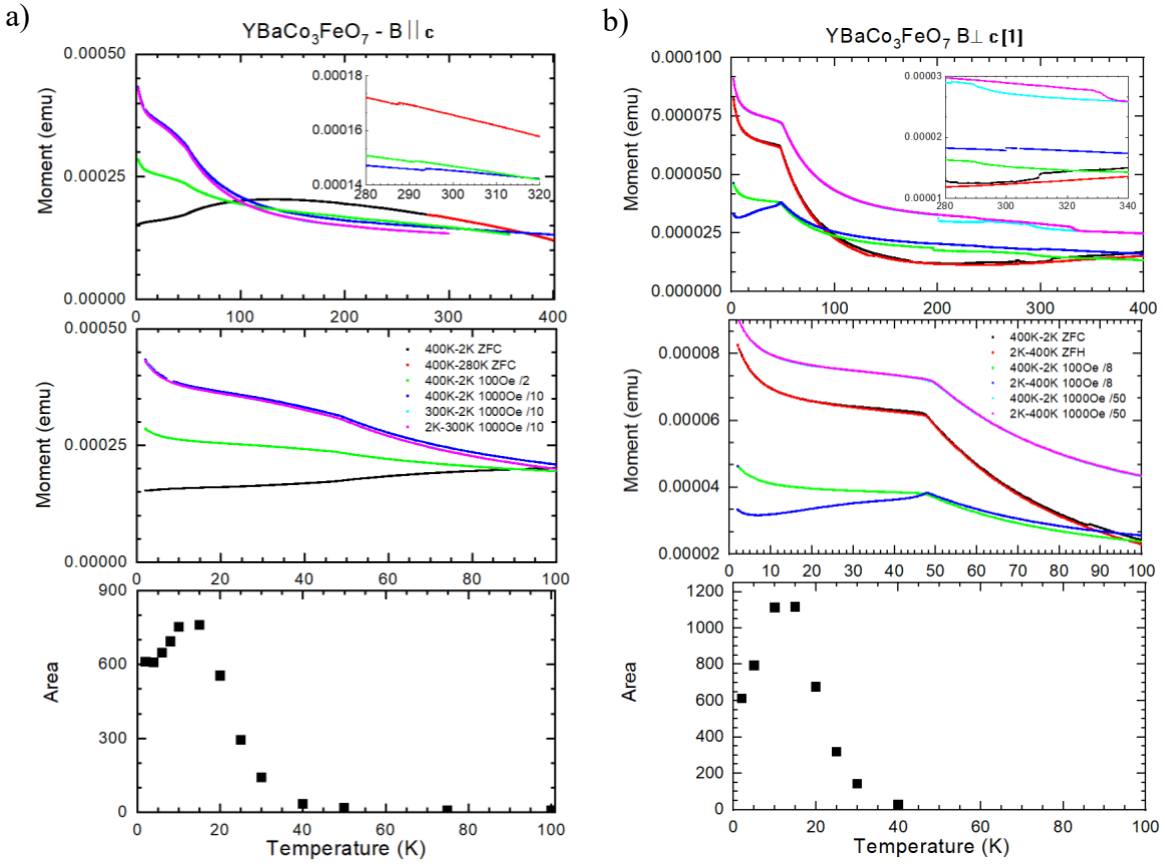


Figure 4.1: *Magnetization measurements and area of the hysteresis loops. The top two graphs show magnetization measurements. The broad continuous transition at 50 K is clearly visible. A further small, sharp step at around 300 K indicates a second magnetic phase transition. Both transitions are in good agreement with previous publications. The lower graph is a temperature-dependent representation of the area under the hysteresis loops. (a) denotes the measurements in the parallel orientation whereas (b) denotes the measurements in the perpendicular [1] orientation.*

Figure 4.2 shows the clear advantage of using a SQUID magnetometer for this experiment. While the hysteresis loops are so small they are barely visible at full scale, the precise measurements of the SQUID as well as the extended field range of $\pm 70{,}000\ Oe$ make a detailed analysis of the hysteresis possible. Again, it should be noted that the hysteresis is most pronounced in both perpendicular orientations, while past experiments have only observed the hysteresis in the parallel orientation, though these findings were based on a much smaller applied field.

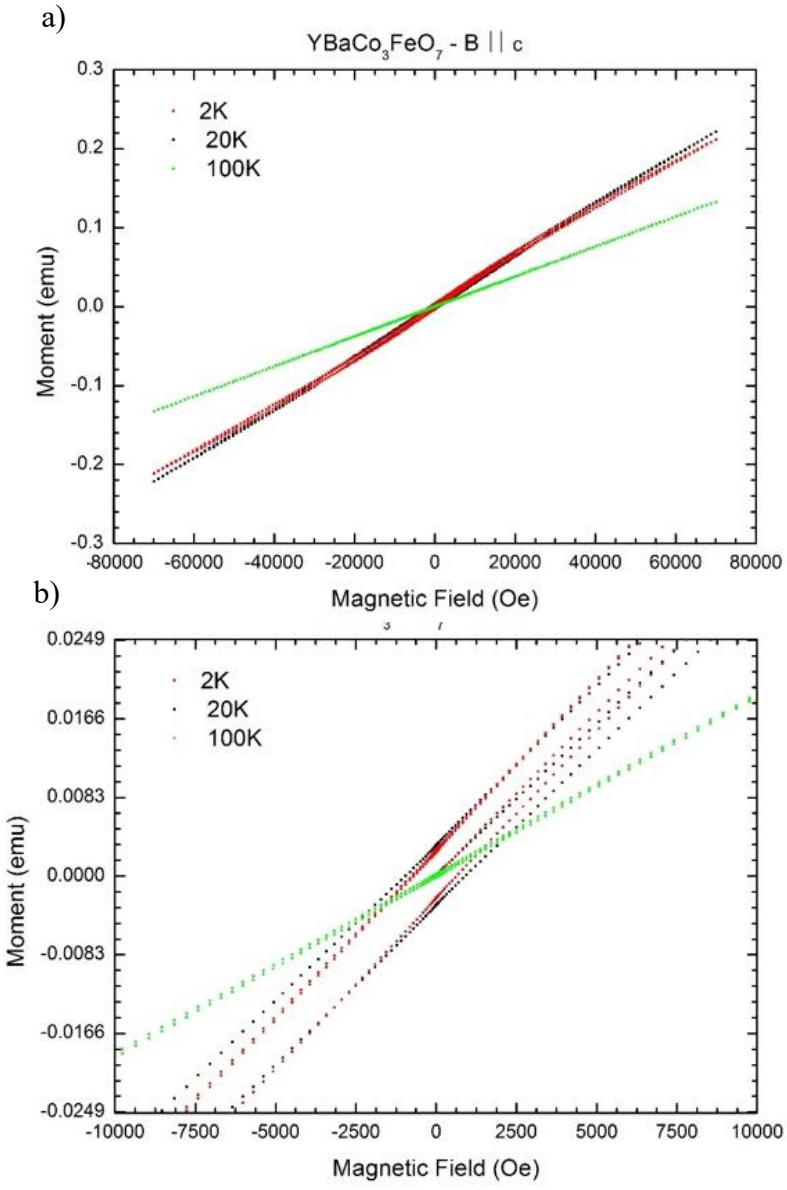


Figure 4.2: *Unprocessed hysteresis loops measured in the parallel orientation with a strong external field of up* $\pm 70{,}000\ Oe$*. For a better overview only the data taken at three different temperatures are shown. (a) visual representation of the hysteresis loops within the entire magnetic field range. The differences between the measurement with increasing and with decreasing magnetic field can barely be seen at this scale. (b) Zoomed in hysteresis loops close to zero applied field. The measurement taken at 20 K clearly yields the biggest differences.*

These findings invite for further analysis of the hysteresis data. For figure 4.3, the lower branch of each hysteresis loop was subtracted from the upper branch at each temperature, essentially yielding a field-dependent representation of the magnitude of the hysteresis. This is possible because the horizontal components of the upper and the lower branch match

precisely, enabling a direct comparison between their vertical values. The rapid decrease in area above 20K can again be witnessed, with the hysteresis becoming essentially insignificant above 50K. It is also noteworthy that the hysteresis consists of two peaks instead of one - this double peak structure indicates more complex magnetic correlations, i.e. at least two different spin ordering processes at work. This could suggest that geometric frustration is not the only reason for the lack of order, but that other quantum processes also contribute to the phenomenon.

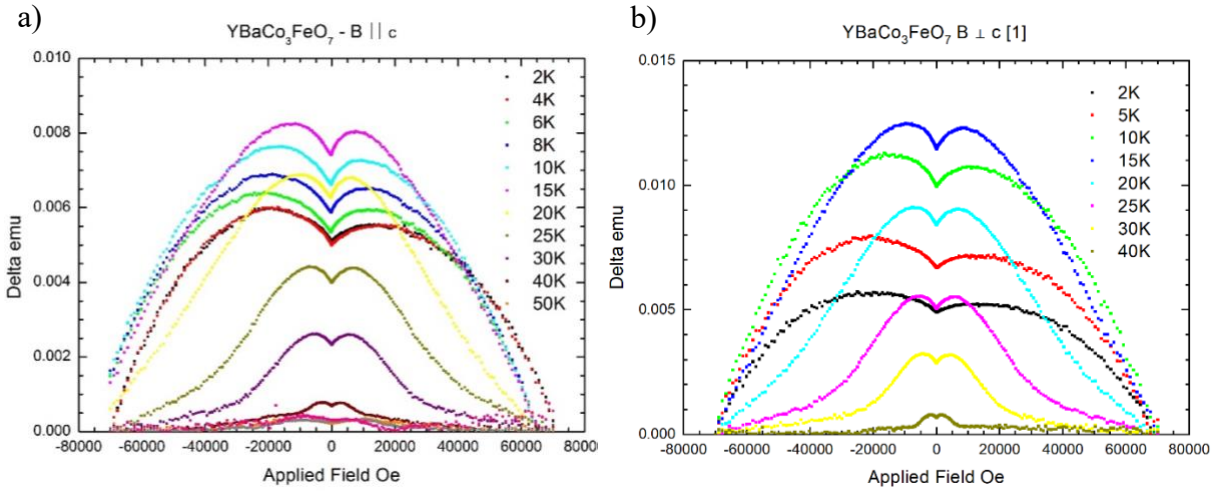


Figure 4.3: *Temperature-dependent representation of the difference of the upper and lower branch of the hysteresis loops. Usually expected is a single symmetric peak with a maximum at zero field. (a) parallel orientation. (b) first perpendicular orientation, which showcases a more pronounced hysteresis.*

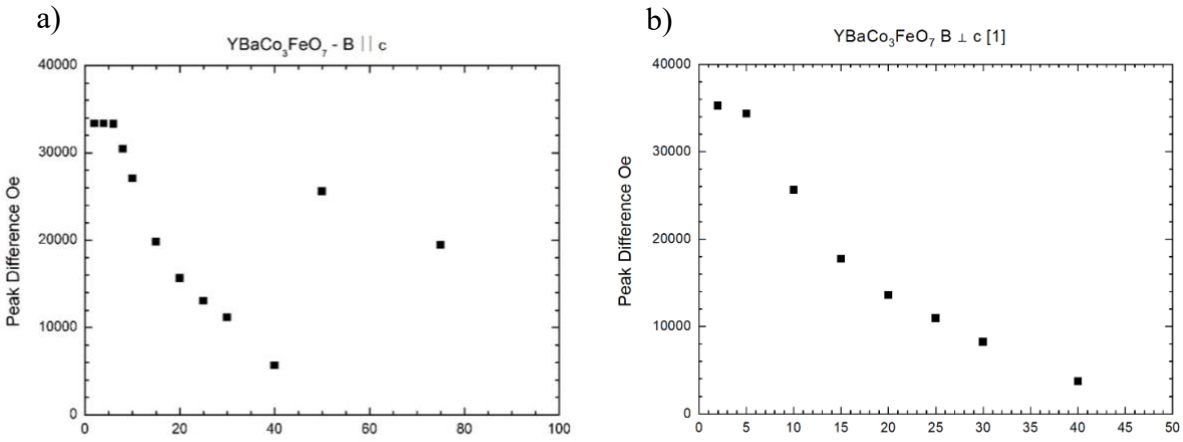


Figure 4.4: *Plot of the peak separation as a function of temperature. Their separation decreases continuously up to about 50 K where it increases step-like, matching the phase transition at that temperature. (a) parallel orientation up to 75K. (b) first perpendicular orientation up to 40K. Unfortunately, data for above 40K could not be obtained in time, so the step-like increase at 50K could only be confirmed in the parallel orientation. However, the similar shape and magnitude in the first perpendicular orientation most likely indicates analogous behavior.*

Another interesting observation is the temperature-dependent behavior of the double peaks. As figure 4.4 shows, the sepeartion between them appears to decrease with an increase in temperature, though behavior above 40K becomes more difficult to see from this graph. To evaluate this, the horizontal components of each peak were estimated by hand and the difference between them was plotted with respect to temperature in figure 4.4. Indeed, it appears that the peak seperation decreases until 40K, with a sharp increase at 50K, from which point the seperation seems to decrease again, although data at these temperatures is more difficult to obtain due to the decreasing magnitude of the hysteresis.

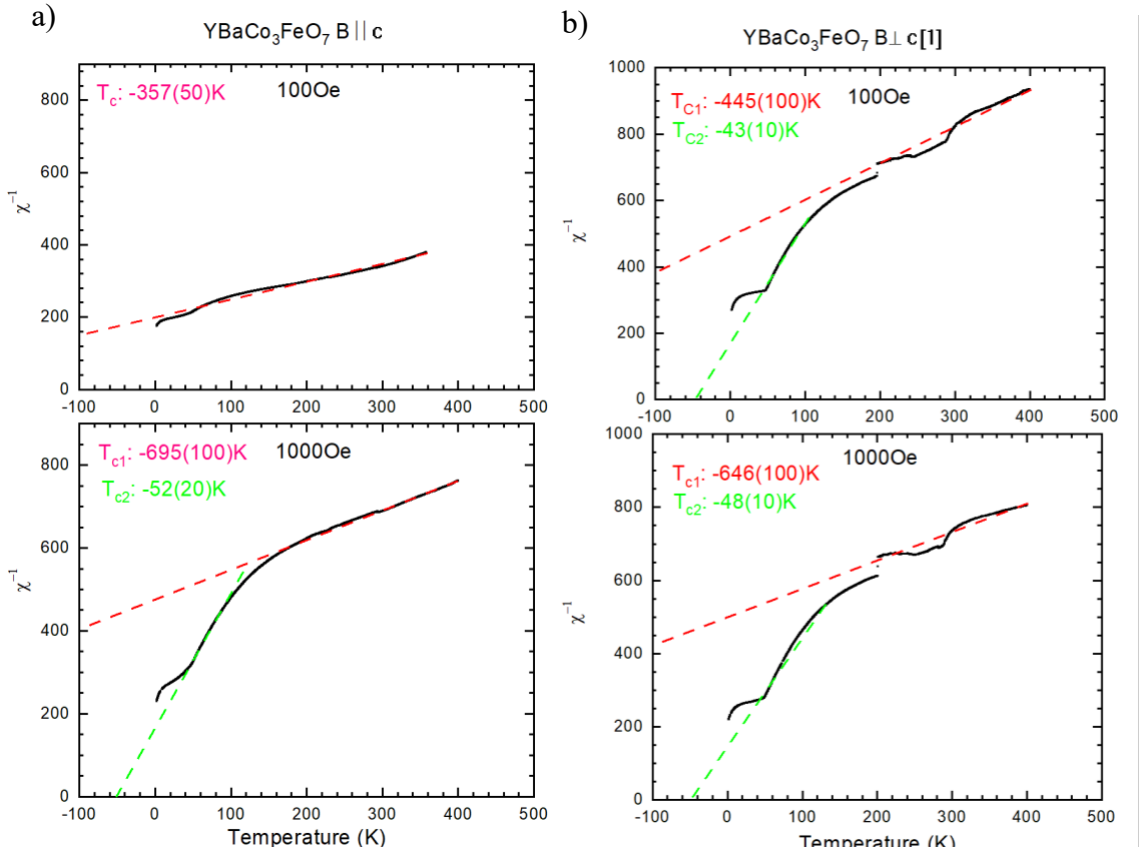


Figure 4.5: *Hand-drawn extrapolation of Curie-Weiss Temperature at 100Oe and 1000Oe applied external field. ZFC estimates do not make sense. Estimates were normed to 1000Oe, meaning that all 100Oe datapoints were multiplied by 10 to account for the difference in external magnetic field. (a) parallel orientation. (b) first perpendicular orientation, matching parallel estimates relatively closely. Two distinct curie temperatures were found in most cases.*

Figure 4.5 shows the Curie-Weiss estimates for the parallel and the first perpendicular orientation. When averaging the lower estimate over all orientations, a Curie-Weiss temperature of -659(50) K is obtained, with the higher estimate at -40(10) K. Both results indicate an anti-ferromagnetic interaction. The lower result roughly matches what has already been experimentally confirmed, while the higher estimate was not found anywhere in literature and again is remarkably close to 50K, the temperature of the transition.

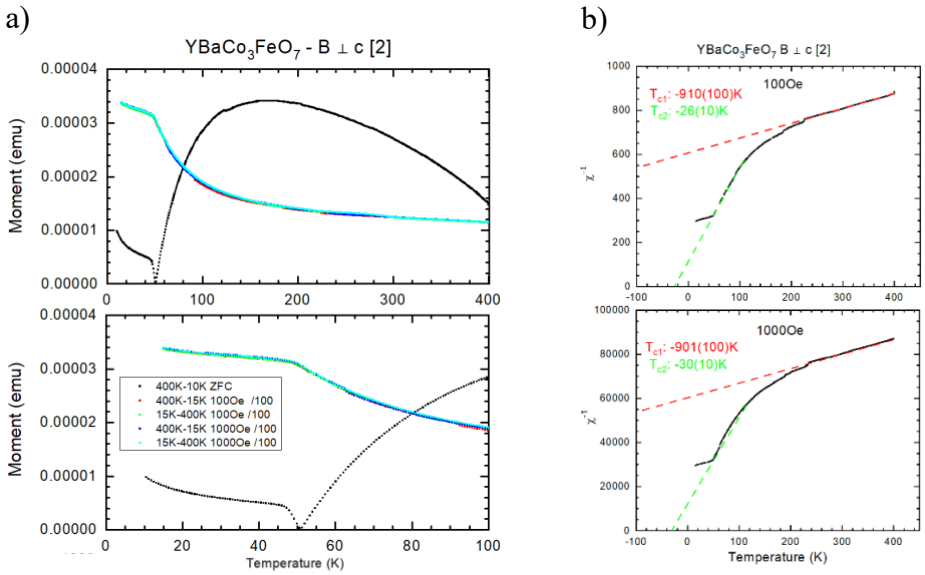


Figure 4.6: *Brief summary of the results in the second perpendicular orientation. (a) shows magnetization measurements and temperature-dependent area of the hysteresis as discussed before. (b) shows Curie-Weiss estimates which were used to extrapolate the average Curie-Weiss temperature.*

As previously mentioned, there was not enough time to complete extensive measurements of the second perpendicular orientation, which is why these results have not been discussed in-depth so far. Temperature-dependent measurements again confirm the transition at 50K, although the disparity in shape between the two perpendicular orientations is striking. This suggests there are some serious differences when measuring the two perpendicular orientations, which is also hinted at by the Curie-Weiss estimates as they significantly deviate from existing findings. A thorough analysis of this orientation would therefore be paramount when trying to fully understand the material system.

5.1 Conclusion

In this experimental analysis, we have performed highly sensitive SQUID magnetization measurements on the geometrically frustrated material $YBaCo_3FeO_7$. According to previous publications, the geometric frustration arising from the crystalline structure results in a spin liquid ground state, though “no true phase transition between the paramagnetic state and the ground state takes place” [1].

Overall, the results obtained here support this conclusion. Though the temperature-dependent measurements indicate sharper transitioning that previously seen (especially with the magnetic field applied perpendicular to the crystallographic c-axis), no true phase transition takes place.

The Curie-Weiss analysis imply that at least two separate ordering processes occur, which is expected, as short-range order was hypothesized previously. Two distinct negative Curie-Weiss temperatures were found, indicating an antiferromagnetic nature. The second temperature at -40(10)K again supports the transitioning at around 50K.

To extend the existing knowledge, hysteresis loops were measured at lowest temperatures, and up to +/- 70,000 Oe. The hysteresis is tiny and only possible to be measured with the highly sensitive SQUID magnetometer. The area under the Hysteresis is proportional to the magnetic energy required for the spin re-ordering process. The existence of a Hysteresis indicates that despite the spin liquid ground state, weak spin correlations exist in YBaCo3FeO7. The area under the hysteresis, i.e. the dissipated energy reaches a maximum at about 20 K. It is important to note that the difference between the upper and the lower branch is not a single maximum at the origin, but instead two distinct peaks are formed, indicating at least two simultaneous spin ordering processes. These peaks keep moving closer together as temperature increases, up until 50K when they noticeably separate again. There was no significant hysteresis observed above 50K.

Using the obtained results, we have been able to confirm and expand the knowledge in this highly exciting, geometrically frustrated spin system. The material in question indeed appears to adopt a spin liquid ground state, although short range ordering still takes place below 50K as demonstrated by the presence of the hysteresis.

5.2 Outlook

Though this investigation has led to some interesting discoveries within the given material system, there are a variety of measurements which could still contribute to a better understanding. First and foremost, measurements in the second perpendicular orientation could not be completed, meaning that a temperature-dependent analysis of the hysteresis, as conducted in the other orientations, was not possible. Such an investigation would be

particularly interesting since the shape of the temperature-dependent magnetization measurements in this orientation significantly differ from what is seen in the first perpendicular orientation, so a hysteresis analysis could contribute to explaining these discrepencies.

Secondly, the temperature range of the hysteresis measurements could be extended upwards in all orientations. This could help confirm the transition at 50K, but also reveal details about the small transition seen around 300K. As the double peak of the hysteresis indicates that geometric frustration may not be the only reason for the lack of order, it is entirely possible that such an analysis could shed light on other interesting features of the crystal.

Finally, the ability to apply an even larger external magnetic field would allow for the hysteresis loops to reach saturation, which has not occurred within the scope of this experiment. Unfortunaely, the SQUID present is not capable of fields stronger than 7T, so another method may be required.

References

[1] W. Schweika et al. “Chiral Spin Liquid Ground State in $YBaCo_3FeO_7$”. Physical Review X 12 (04. May 2022). DOI: 10.1103/PhysRevX.12.021029.

[2] M. Valldor et. al. “Spin Correlations in the Extended Kagome System $YBaCo_3FeO_7$”. Physical Review B 84 (22. Dec 2011) DOI: PhysRevB.84.224426.

[3] C. Byrne. “A Brief History of Electromagnetism”. Department of Mathematical Sciences, University of Massachutas Lowell (02. Jan 2015). https://faculty.uml.edu/cbyrne/EMHIST.pdf

[4] L. Chu et al. “Electron Spin”. LibreTexts Chemistry (03. Oct 2023). https://chem.libretexts.org/@go/page/1651

[5] M. Malki et al. “A Multiphysics Thermoelastoviscoplastic Damage Internal State Variable Constitutive Model including Magnetism”. Materials (17. May 2024). DOI: 10.3390/ma17102412

[6] Textbook.com. “What is Hysteresis? - Learn the Concept in Detail!”. Textbook.com (14. June 2024). https://testbook.com/physics/hysteresis

[7] S. Arar. “Understanding Magnetic Field Energy and Hysteresis Loss in Magnetic Cores”. All About Circuits (26. June 2024). https://www.allaboutcircuits.com/technical-articles/understanding-magnetic-field-energy-and-hysteresis-loss-in-magnetic-cores/

[8] K. Yokosawa. “Overview of Magnetoencephalography—Brief History of its Sensors and Hardware”. J-Stage (December 2020). DOI: 10.14326/abe.9.217

[9] Quantum Design. “SQUID Magnetometer – Quantum Design MPMS3”. Quantum Design. https://www.qdusa.com/products/mpms3.html

[10] M. Valdor and O. Breuning. “Crystal Structure and Properties of the Manganese Containing Swedenborgite $YBaMn_3AlO_7$”. Solid State Sci. 13 (2011). DOI: 10.1016/J.SOLIDSTATESCIENCES.2011.03.014

[11] M. Valldor. “Syntheses and Structures of Compounds with $YBaCo_3FeO_7$-Type Structure”. Solid State Sci. 6 (2004). DOI: 10.1016/j.solidstatesciences.2004.01.004